Formation Mechanism of FePt Nanoparticles Synthesized via Pyrolysis of Iron(III) Ethoxide and Platinum(II) Acetylacetonate

Soichiro Saita[†] and Shinya Maenosono*[,‡]

Mitsubishi Chemical Group Science and Technology Research Center, Incorporated (MCRC), Kamoshida-cho, Aoba-ku, Yokohama, Kanagawa 227-8502, Japan, and Department of Chemical System Engineering, School of Engineering, The University of Tokyo, Hongo 7-3-1, Bunkyo-ku, Tokyo 113-8656, Japan

Received August 7, 2005. Revised Manuscript Received September 27, 2005

In this study the mechanism for the formation of FePt nanoparticles (NPs) via the pyrolysis of iron(III) ethoxide [$Fe(OEt)_3$] and platinum(II) acetylacetonate [$Pt(acac)_2$] is investigated. We have recently reported that monodispersed equiatomic FePt NPs with a mean diameter of 4.5 nm and a narrow composition distribution were successfully synthesized by this route. However, control of the mean size and further narrowing of the size distribution have not yet been achieved. In the present study, we systematically examined variability in the particle size D_p, size distribution σ, and atomic composition of the NPs with changing synthetic conditions such as reaction temperature, rate of temperature increase, and total amounts and input molar ratios of precursors and capping agents. As a result, D_p was varied from 1.8 to 6.8 nm, the best size distribution σ achieved was 16%, and the Fe content of the NPs varied from 29 to 51 atomic %. On the basis of the experimental results, we determined the following important aspects of the reaction mechanism: (i) The FePt NPs are rapidly formed at 250−297 °C by the allelocatalytic decomposition of precursors. (ii) The formation of FePt NPs is dominated by nucleation of Pt followed by a slow growth process of Fe (and Pt) atoms. (iii) Fe and Pt atoms are stabilized by oleic acid and oleylamine, respectively.

Introduction

$L1_0$ FePt nanoparticles (NPs) have a large magnetocrystalline anisotropy and, thus, exhibit large coercivity at room temperature, even when their size is as small as several nanometers.[1] After the IBM group reported the synthesis of FePt NPs in a liquid phase using iron pentacarbonyl [$Fe(CO)_5$] and platinum(II) acetylacetonate [$Pt(acac)_2$] as precursors,[2] numerous groups investigated advanced synthetic methods for FePt NPs.[3] FePt NPs have been intensively studied for many applications such as high-density recording media[2,4] and ferromagnetic nanocomposites.[5] Undesirable sintering between NPs, which takes place when NPs are annealed to transform the crystalline structure from the chemically disordered face-centered cubic (fcc) to the chemically ordered $L1_0$ phase (face-centered tetragonal), should be avoided.[6] In view of this, it would be convenient if independently isolated ferromagnetic $L1_0$ FePt NPs could be obtained for self-assembly of NPs into two-dimensional or three-dimensional arrangements with a *c*-axis orientation[7] or for attaching various ligand molecules on the surface of NPs to improve functionality. Although $L1_0$ FePt NPs can be synthesized directly using a polyol reduction method at high temperatures, the resulting NPs often tend to aggregate[8] and the quality of FePt NPs is inferior to those obtained by using $Fe(CO)_5$. To obtain independently isolated ferromagnetic FePt NPs, the atomic composition of each single NP should be within 40−60% Fe to allow transformation into the $L1_0$ phase.[9] Additionally, the diameter of NPs (D_p) should be larger than the superparamagnetic limit of $L1_0$ FePt (ca.

* Corresponding author. E-mail: shinya@chemsys.t.u-tokyo.ac.jp.
[†] MCRC.
[‡] The University of Tokyo.

(1) (a) Sun, S.; Fullerton, E. E.; Weller, D.; Murray, C. B. *IEEE Trans. Magn.* **2001**, *37*, 1239. (b) Weller, D.; Moser, A. *IEEE Trans. Magn.* **1999**, *35*, 4423.
(2) Sun, S.; Murray, C. B.; Weller, D.; Folks, L.; Moser, A. *Science* **2000**, *287*, 1989.
(3) (a) Teng, X.; Yang, H. *J. Am. Chem. Soc.* **2003**, *125*, 14559. (b) Nakaya, M.; Tsuchiya, Y.; Ito, K.; Oumi, Y.; Sano, T.; Teranishi, T. *Chem. Lett.* **2004**, *33*, 130. (c) Kang, S. S.; Nikles, D. E.; Harrell, J. W. *J. Appl. Phys.* **2003**, *93*, 7178. (d) Reiss, B. D.; Mao, C.; Solis, D. J.; Ryan, K. S.; Thomson, T.; Belcher, A. M. *Nano Lett.* **2004**, *4*, 1127. (e) Harpeness, R.; Gedanken, A. *J. Mater. Chem.* **2005**, *15*, 698.
(4) (a) Christodoulides, J. A.; Zhang, Y.; Hadjipanayis, G. C.; Fountzoulas, C. *IEEE Trans. Magn.* **2000**, *36*, 2333. (b) Kodama, H.; Momose, S.; Ihara, N.; Uzumaki, T.; Tanaka, A. *Appl. Phys. Lett.* **2003**, *83*, 5253.
(5) (a) Mazaleyrat, F.; Varga, L. K. *J. Magn. Magn. Mater.* **2000**, *215*−*216*, 253. (b) Rong, C. B.; Zhang, H. W.; Du, X. B.; Zhang, J.; Zhang, S. Y.; Shen, B. G. *J. Appl. Phys.* **2004**, *96*, 3921. (c) Gan'shina, E.; Aimuta, K.; Granovsky, A.; Kochneva, M.; Sherbak, P.; Vashuk, M.; Nishimura, K.; Inoue, M. *J. Appl. Phys.* **2004**, *95*, 6882.
(6) (a) Jeyadevan, B.; Hobo, A.; Urakawa, K.; Chinnasamy, C. N.; Shinoda, K.; Tohji, K. *J. Appl. Phys.* **2003**, *93*, 7574. (b) Ding, Y.; Majetich, S. A.; Kim, J.; Barmak, K.; Rollins, H.; Sides, P. *J. Magn. Magn. Mater.* **2004**, *284*, 336.
(7) Kodama, H.; Momose, S.; Sugimoto, T.; Uzumaki, T.; Tanaka, A. *IEEE Trans. Mag.* **2005**, *41*, 665.
(8) (a) Jeyadevan, B.; Urakawa, K.; Hobo, A.; Chinnasamy, N.; Shinoda, K.; Tohji, K.; Djayaprawira, D. D.; Tsunoda, M.; Takahashi, M. *Jpn. J. Appl. Phys.* **2003**, *42*, L350. (b) Sato, K.; Jeyadevan, B.; Tohji, K. *J. Magn. Magn. Mater.* **2005**, *289*, 1. (c) Kang, S.; Jia, Z.; Shi, S.; Nikles, D. E.; Harrell, J. W. *Appl. Phys. Lett.* **2005**, *86*, 62503. (d) Takahashi, M.; Ogawa, T.; Hasegawa, D.; Jeyadevan, B. *J. Appl. Phys.* **2005**, *97*, 10J307. (e) Kang, S.; Jia, Z.; Shi, S.; Nikles, D. E.; Harrell, J. W. *J. Appl. Phys.* **2005**, *97*, 10J318.
(9) Stahl, B.; Ellrich, J.; Theissmann, R.; Ghafari, M.; Bhattacharya, S.; Hahn, H.; Gajbhiye, N. S.; Kramer, D.; Viswanath, R. N.; Weissmuller, J.; Gleiter, H. *Phys. Rev. B* **2003**, *67*, 14422.

10.1021/cm051760h CCC: $30.25
Published on Web 11/23/2005

3.3 nm).[10] For well-ordered two-dimensional or three-dimensional assembly, the size distribution (σ) should generally be below 10%.[11] Moreover, it is necessary to transform as-synthesized chemically disordered fcc FePt NPs into the chemically ordered $L1_0$ phase while avoiding severe sintering and aggregation.

There are a number of technological difficulties that must be overcome to meet these requirements. For example, mean size control, in which a desirable average composition and uniformity of NPs is attained, is still a big challenge. Momose et al. have reported that D_p can be successfully varied from 2.1 to 4.3 nm by changing the input amount of capping agents, based on the synthetic route first proposed by the IBM group, in which $Fe(CO)_5$ and $Pt(acac)_2$ are used as precursors.[12] Chen et al. have synthesized FePt NPs with D_p values of up to 9 nm in size by precisely controlling the reaction conditions, such as the kind of solvent used, the amount of capping agent, the temperature, the rate of temperature increase, and the reaction time.[13] However, in general, it is difficult to synthesize FePt NPs with D_p values larger than 5 nm and uniform size and composition distributions.

Yu et al. have recently clarified that FePt NPs synthesized via the IBM method have a wide composition distribution, even though the atomic composition of Fe should be within 40 to 60 atomic % Fe, if independently isolated ferromagnetic FePt NPs are to be obtained.[14] They analyzed more than 100 individual FePt NPs by energy dispersive X-ray (EDX) spectrometry and found that only around 29.0% of the Fe_xPt_{100-x} NPs were within the composition range of $40 < x < 60$, while approximately 40.5 and 30.5% of the NPs were Pt-rich and Fe-rich, respectively. Because a major portion of $Fe(CO)_5$ exists in the vapor phase because the boiling point of $Fe(CO)_5$ is much lower than the decomposition temperature and vapor-phase $Fe(CO)_5$ is continuously supplied to the liquid phase by reflux during the reaction, a significant spatio-temporal inhomogeneity of the $Fe(CO)_5$ concentration results in the reaction system. This could be the reason for the broad composition distribution of NPs.

We have recently reported the synthesis of FePt NPs using iron(III) ethoxide [$Fe(OEt)_3$] and $Pt(acac)_2$ as precursors without any reducing agent to overcome some of the above-mentioned difficulties.[15] $Fe(OEt)_3$ is a highly reactive late transition metal alkoxide that is hard to oxidize, easy to handle, and not very toxic. Equiatomic FePt NPs of 4.5 nm average diameter with a good composition distribution have been obtained by this synthetic method. The fraction of Fe_xPt_{100-x} NPs which were within an appropriate composition range for transformation into the $L1_0$ phase was found to be over 70%. The reason for the narrowing of the composition distribution was thought to be related to synchronization between the thermal decomposition of $Fe(OEt)_3$ and the reduction of $Pt(acac)_2$. However, mean size control and further narrowing of the size distribution range have not yet been achieved. In addition, the reaction mechanism of this synthesis method is almost completely unknown. To obtain high-quality FePt NPs via this synthetic route and to further control the size, composition, and size distribution, a better understanding of the reaction mechanism is required. Hence, in the present study, we systematically investigated the variability in the particle size D_p, size distribution σ, and atomic composition of NPs that is obtained by changing synthetic conditions such as the reaction temperature, rate of temperature increase, and total amounts and input molar ratios of precursors and capping agents.

Experimental Section

FePt NP Synthesis. Iron(III) ethoxide [$Fe(OEt)_3$, purity 95%] was purchased from AZmax. Platinum(II) acetylacetonate [$Pt(acac)_2$, purity 97%] was purchased from Strem Chemicals. Octyl ether (purity 99%), oleic acid (90%) and oleylamine (70%) were purchased from Aldrich. All reagents were used without further purification. The standard synthesis conditions were as follows. A total of 1 mmol of $Fe(OEt)_3$, 0.5 mmol of $Pt(acac)_2$, 17 mL of octyl ether, 5 mmol of oleic acid, and 5 mmol of oleylamine were placed in a three-necked round-bottom flask under ambient air. The molar ratio of Fe to Pt and the fraction of oleic acid to the total amount of capping agent in the mother reaction solution were adjusted to 2 and 0.5, respectively, in the standard conditions. Note that no reducing agent was used. The flask was then evacuated to remove oxygen and volatile components from the reaction solution. After evacuation, the flask was purged three times by high-purity Ar. Subsequently, the temperature was raised to 297 °C at a rate of 20 °C/min under an Ar atmosphere. At around 150 °C, white smoke billowed from the solution and the reactant gradually turned black. After 30 min of reaction at 297 °C, the flask was cooled to 50 °C and ethanol that had N_2 bubbled through it was added to the flask. By centrifuging this mixture, a black powder was separated from the matrix. The powder was then redispersed in hexane. Precipitation and redispersion processes were repeated three times to completely remove impurities. By this synthetic procedure, 50 mg of FePt NPs capped with oleic acid were obtained. The average composition of FePt NPs was determined by inductively coupled plasma atomic emission spectrometry (ICP-AES; Jobin Yvon JY38-S).

Several samples were synthesized using conditions that differed from the above-mentioned standard conditions. First, the input molar ratio of Fe to Pt was varied to 1, 2, and 3 by changing the amount of $Fe(OEt)_3$ from 0.5 to 1.5 mmol while the other conditions were kept identical to the standard conditions. Second, the total amount of precursors [$Fe(OEt)_3 + Pt(acac)_2$] was varied to 0.75, 1.5, and 3 mmol by fixing the Fe/Pt molar ratio at 2/1 while the other conditions were kept identical to the standard conditions. Finally, the input molar fraction of oleic acid $O_{ac}/(O_{ac} + O_{am})$ was varied to 0.25, 0.5, 0.67, 0.75, and 1 while fixing $O_{ac} + O_{am} = 10$ mmol, where O_{ac} and O_{am} are the input amounts of oleic acid and oleylamine, respectively.

X-ray Photoelectron Spectroscopy (XPS). XPS analysis was carried out by a PHI Quantum 2000 scanning ESCA microprobe. Photoelectrons were excited by monochromated Al Kα radiation and detected with a concentric hemispherical analyzer (CHA). An X-ray tube was operated at 30 W. The pass energy of the CHA

(10) Weller, D.; Moser, A.; Folks, L.; Best, M. E.; Lee, W.; Toney, M. F.; Schwickert, M.; Thiele, J. U.; Doerner, M. F. *IEEE Trans. Magn.* **2000**, *36*, 10.
(11) (a) Lacks, D. J.; Wienhoff, J. R. *J. Chem. Phys.* **1999**, *111*, 398. (b) Auer, S.; Frenkel, D. *Nature* **2001**, *413*, 711.
(12) Momose, S.; Kodama, H.; Uzumaki, T.; Tanaka, A. *Jpn. J. Appl. Phys.* **2005**, *44*, 1147.
(13) Chen, M.; Liu, J. P.; Sun, S. *J. Am. Chem. Soc.* **2004**, *126*, 8394.
(14) Yu, A. C. C.; Mizuno, M.; Sasaki, Y.; Kondo, H. *Appl. Phys. Lett.* **2004**, *85*, 6242.
(15) Saita, S.; Maenosono, S. *Chem. Mater.* **2005**, *17*, 3705.

was 29.35 eV for narrow-scan spectra. The analyzed area on the specimen surface was 500 × 500 μm^2 and was located in the center of the irradiated region. For the sample preparation, FePt NPs were dispersed in hexane and spin-casted on a silicon substrate in a nitrogen glovebox.

X-ray Diffractometry (XRD) and Transmission Electron Microscopy (TEM). XRD patterns of FePt NPs were obtained in the reflection geometry using an X-ray diffractometer (Rigaku, RINT200PC) at room temperature with Cu Kα radiation (wavelength, 1.542 Å; incident angle, 1°; step width, 0.05°; counting time, 1 s). FePt NPs were deposited on glass substrates for XRD measurements (Matsunami Micro Slide Glass, 8 × 10 mm^2) by casting and drying the NP/hexane dispersion. High-resolution TEM micrographs and selected-area electron diffraction (SAED) patterns of FePt NPs were obtained using a Hitachi H-9000UHR microscope operated at 300 kV. The average size D_p and size distribution σ of thr FePt NPs was estimated from over 300 randomly selected NPs from the TEM images.

Thermal Analysis. Thermogravimetry−differential thermal analysis (TG-DTA; Seiko, TG/DTA320) was performed using an electrical furnace, to investigate the thermal decomposition behavior of precursors (Seiko Instruments, SSC/5200). Three milligram quantities of $Fe(OEt)_3$ or $Pt(acac)_2$ or a mixture of these was placed in a quartz cell, and this was then placed in a furnace. The temperature was raised to 1000 °C at a heating rate of 20 °C/min under a N_2 atmosphere (flow rate 200 mL/min). The heating rate was conformed to that of the synthesis. The mixture samples were prepared by dissolving appropriate amounts of $Fe(OEt)_3$ and $Pt(acac)_2$ in ethanol, followed by gradual drying of the solutions. Thermogravimetry−mass spectrometry (TG-MS; Shimazu, TGMS-direct) was also carried out to determine the decomposition products of the precursors. Three milligram quantities of $Fe(OEt)_3$ or $Pt(acac)_2$ or a mixture of these was placed in a quartz cell, and the temperature was raised to 1000 °C at a heating rate of 20 °C/min under a He atmosphere (flow rate 100 mL/min). The decomposition products were then analyzed by MS.

Results

Effects of Rate of Temperature Increase and Reaction Time. Chen et al. have reported that the mean diameter of FePt NPs (D_p) strongly depends on the rate of temperature increase during synthesis.[13] In their work, when the rate of temperature increase is small, D_p becomes large. Their result is consistent with results obtained for FeMo[16] and $CoPt_3$[17] systems. In each case, by tuning the rate of the temperature increase, the reaction temperature or the reaction time, the degree of supersaturation could be controlled, and thus D_p and the size distribution (σ) were successfully varied. Consequently, we attempted to vary D_p and σ by changing the rate of temperature increase in the present synthesis, in which $Fe(OEt)_3$ is used as a precursor, expecting similar effects. We varied the rate of temperature increase from 3 to 20 °C/min. The reaction temperature was fixed at 297 °C, and the reaction time (t_R), that is, the length of time for which the reaction was allowed to continue after the reaction temperature had been reached, was fixed at t_R = 30 min. However, changing the rate of temperature increase did not result in a significant difference in the size of synthesized FePt NPs. This result suggests that the mechanism for the formation of FePt NPs via the current method is quite different from the mechanism(s) for the other synthetic methods.

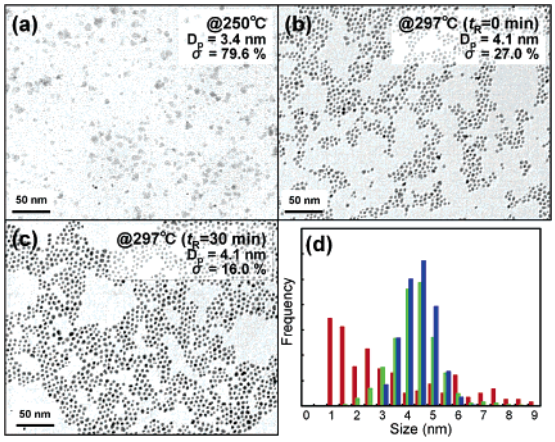

Figure 1. TEM micrographs of as-synthesized NPs taken when the temperature reached (a) 250 and (b) 297 °C (t_R = 0 min) and (c) after the reaction at standard conditions (t_R = 30 min). The rate of temperature increase was 20 °C/min. (d) Size distributions of each sample. Red, green, and blue histograms correspond to the distributions of parts a, b, and c, respectively.

In the next set of experiments, the reaction temperature was set to 100 or 150 °C, with t_R = 2 h (the rate of temperature increase was fixed at 20 °C/min). No FePt NPs were formed in these low-temperature reactions. Thus, we next carried out a synthesis in which the reaction temperature was set at 297 °C and took samples while the temperature was still rising (at 250 °C) and at the reaction temperature (297 °C). The sample taken at 250 °C contained atypical NPs of D_p = 3.4 nm as shown in Figure 1a. However, these NPs were not FePt but γ-Fe_2O_3 (or Fe_3O_4), because the peaks corresponding to fcc FePt were absent, and the (311) peak of γ-Fe_2O_3 (or Fe_3O_4) was observed at 2θ = 35.384° in the XRD pattern, as shown in Figure 2a (bottom curve). On the other hand, the sample taken at 297 °C (t_R = 0 min) contained FePt NPs of D_p = 4.1 nm (σ = 27%) as shown in Figure 1b. Curve 2 in Figure 2a corresponds to the XRD pattern of this sample and is representative of typical chemically disordered fcc FePt NPs. These results indicate that the generation of FePt NPs occurred rapidly as the temperature was rising from 250 to 297 °C. On completion of the reaction at standard conditions (t_R = 30 min), FePt NPs of D_p = 4.1 nm (σ = 16%) were obtained, as shown in Figure 1c. The average size of FePt NPs did not increase during the 30 min of reaction at 297 °C. This indicates that the formation process of FePt NPs is dominated by nucleation. Of note is that σ decreased considerably after the 30 min of reaction at 297 °C compared with the sample taken when the temperature had just reached 297 °C (t_R = 0 min), as shown in Figure 1d; on the other hand, D_p did not increase. Curve 3 in Figure 2a shows the XRD pattern of the FePt NPs synthesized under standard conditions and is representative of typical chemically disordered fcc FePt NPs. The (111) and (200) rings of the fcc-phase FePt crystallite were also clearly seen in the SAED pattern (data not shown). We also investigated how reproducible a given condition is with respect to D_p and σ by synthesizing FePt NPs in four batches

(16) Li, Y.; Liu, L.; Wang, Y.; Wang, Z. L. *Chem. Mater.* **2001**, *13*, 1008.
(17) Shevchenko, E. V.; Talapin, D. V.; Schnablegger, H.; Komowski, A.; Festin, O.; Svedlindh, P.; Haase, M.; Weller, H. *J. Am. Chem. Soc.* **2003**, *125*, 9090.

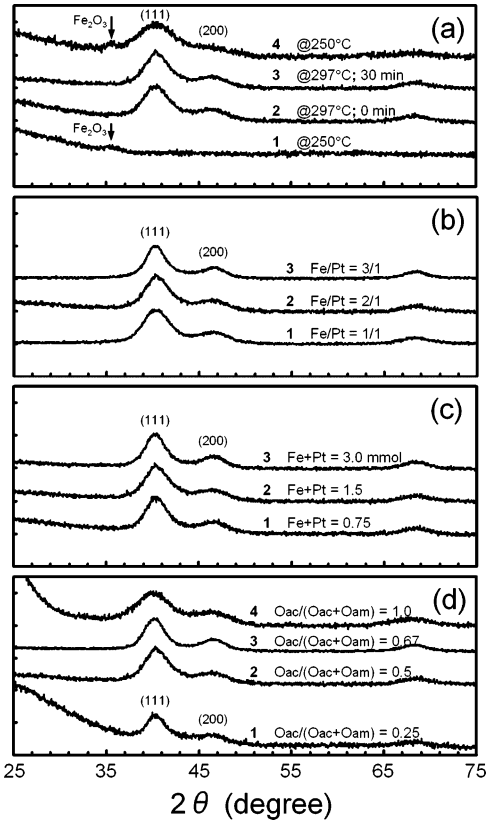

Figure 2. XRD patterns of as-synthesized FePt NPs. (a) XRD patterns of samples taken when the temperature reached 250 (curve 1) and 297 °C (curve 2) ($t_R = 0$ min) and after the reaction under standard conditions ($t_R = 30$ min; curve 3). Curve 4 represents the XRD pattern of a sample synthesized via the pre-decomposition of Fe precursor (see text). (b) XRD patterns of samples synthesized with varying amounts of $Fe(OEt)_3$: 0.5 (curve 1), 1.0 (curve 2), and 1.5 mmol (curve 3). (c) XRD patterns of samples synthesized with varying total amounts of precursors: 0.75 (curve 1), 1.5 (curve 2), and 3 mmol (curve 3). (d) XRD patterns of samples synthesized with varying $O_{ac}/(O_{ac} + O_{am})$ values: 0.25 (curve 1), 0.5 (curve 2), 0.67 (curve 3), and 1.0 (curve 4).

under standard conditions. Average values of D_p and σ were found to be $\bar{D}_p = 4.5$ nm (standard deviation 0.3 nm) and $\bar{\sigma} = 18\%$ (standard deviation 2.2%).

Effects of the Input Fe/Pt Precursor Ratio and the Total Amount of Precursor. From the above results, it appears to be difficult to control D_p by changing the rate of temperature increase or the reaction time. Consequently, we next investigated the effects of the input molar ratio of Fe to Pt (i.e., the Fe/Pt molar ratio added at the start of the reaction) on D_p and σ. Figure 3 shows the TEM micrographs of FePt NPs synthesized with Fe/Pt = 1/1, 2/1 (standard condition), and 3/1 (parts a, b, and c, respectively). The average sizes of the resulting NPs were $D_p = 3.2$ ($\sigma = 19.6\%$), 4.1 ($\sigma = 16\%$), and 5.0 ($\sigma = 29.2\%$) nm, respectively. The average size increased with an increasing Fe/Pt ratio (Figure 3d), and in the case of Fe/Pt = 3/1, the size distribution was considerably broadened and the shape of the NPs was atypical. The XRD patterns of these samples are shown in Figure 2b and are representative of fcc FePt NPs. There was no significant difference between the three XRD patterns. The Fe contents of FePt NPs as measured by ICP-AES were 38, 50, and 51 atomic % for Fe/Pt = 1/1, 2/1, and 3/1, respectively. The Fe content in the NPs was found to be saturated when Fe/Pt ≥ 2. This could be due to

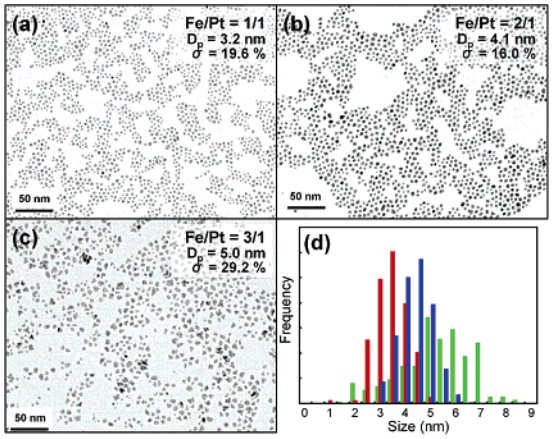

Figure 3. TEM micrographs of FePt NPs synthesized with varying amounts of $Fe(OEt)_3$: (a) 0.5, (b) 1.0, and (c) 1.5 mmol. (d) Size distributions of each sample. Red, blue, and green histograms correspond to the distributions of parts a, b, and c, respectively.

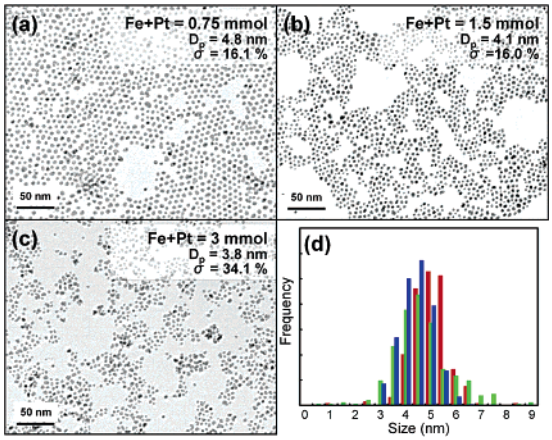

Figure 4. TEM micrographs of FePt NPs synthesized with varying total amounts of precursors [$Fe(OEt)_3 + Pt(acac)_2$]: (a) 0.75, (b) 1.5, and (c) 3 mmol, at a fixed Fe/Pt molar ratio of 2/1. (d) Size distributions of each sample. Red, blue, and green histograms correspond to the distributions of parts a, b, and c, respectively.

an increased level of Pt production with increased amounts of $Fe(OEt)_3$, due to the allelocatalytic effect, which will be discussed in a later section, resulting in a large D_p and Fe content saturation. In addition, the atypical shape of NPs in the case of Fe/Pt = 3/1 may be caused by a deficiency in the amount of oleic acid in comparison to the amount of Fe precursor (details of this will be discussed in the next section).

We then changed the total amount of Fe and Pt precursor (Fe + Pt) while keeping a fixed ratio of Fe/Pt = 2/1. Figure 4 shows the TEM micrographs of FePt NPs synthesized with Fe + Pt = 0.75, 1.5 (standard condition), and 3.0 mmol (parts a, b and c, respectively). The average sizes of NPs were $D_p = 4.8$ ($\sigma = 16.1\%$), 4.1 ($\sigma = 16\%$), and 3.8 ($\sigma = 34.1\%$) nm, respectively. The average size increased with decreasing total amounts of Fe and Pt precursor (Figure 4d). This result could be explained as follows. By decreasing the total amount of precursor, the degree of supersaturation decreases. As a result, the number density of nuclei decreases and the critical size of the nucleus increases. The large σ obtained when Fe + Pt = 3.0 mmol may be caused by a deficiency in the amount of capping agent, as discussed in the next section, and the resulting aggregation among NPs. The XRD patterns

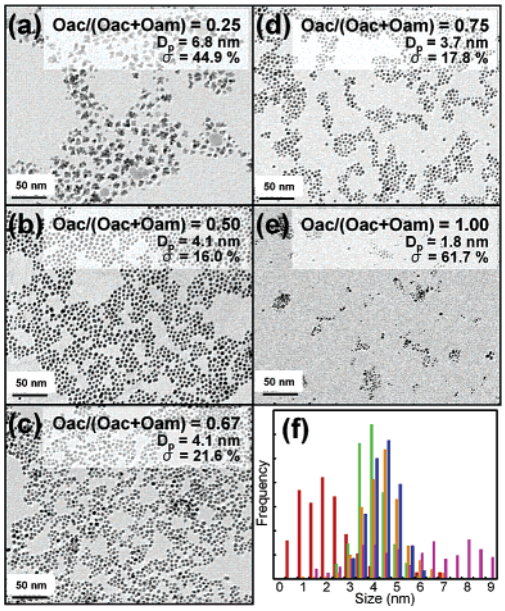

Figure 5. TEM micrographs of FePt NPs synthesized with varying input molar fractions of oleic acid $O_{ac}/(O_{ac} + O_{am})$: (a) 0.25, (b) 0.5, (c) 0.67, (d) 0.75, and (e) 1.0, at a fixed $O_{ac} + O_{am} = 10$ mmol. (f) Size distributions of each sample. Pink, blue, orange, green, and red histograms correspond to the distributions of parts a, b, c, d, and e, respectively.

of these samples are shown in Figure 2c and are representative of fcc FePt NPs.

Effects of Amounts of Oleic Acid and Oleylamine. On the basis of the results described in the previous section, the amount of capping agent present was thought to be an important parameter for controlling D_p and σ. In similar work on FeMo NP synthesis, D_p and σ values of NPs varied significantly when the molar ratio of octanoic acid to bis-2-ethylhexylamine (i.e., the molar ratio of one capping agent to another) was varied.[16] To investigate the roles of oleic acid and oleylamine in the present reaction, we changed the input molar fraction of oleic acid $O_{ac}/(O_{ac} + O_{am})$ while fixing the total amount of capping agent, $O_{ac} + O_{am} = 10$ mmol, where O_{ac} and O_{am} are the input amounts of oleic acid and oleylamine, respectively. Figure 5 shows the TEM micrographs of FePt NPs synthesized with $O_{ac}/(O_{ac} + O_{am}) = 0.25$, 0.5 (standard condition), 0.67, 0.75, and 1 (parts a, b, c, d, and e, respectively). Figure 5f shows the size distributions of each sample. When $O_{ac}/(O_{ac} + O_{am}) = 1$, that is, $O_{am} = 0$ mmol, ultrafine FePt NPs of $D_p = 1.8$ nm ($\sigma = 61.7\%$) were obtained. The XRD pattern of this sample is shown in Figure 2d (curve 4). Significant broadening of the (111) and (200) peaks is observed because of the ultrasmall crystalline size. The mean crystallite size, estimated from the full width at half-maximum of the (111) peak by the Scherrer formula, (D_{xrd}), was 1.94 nm. The composition of obtained FePt NPs was determined to be $Fe_{29}Pt_{71}$ by ICP-AES. This result suggests that Fe atoms produced by the decomposition of $Fe(OEt)_3$ were stabilized by oleic acid molecules, and, therefore, the Fe intake into the NPs decreased.

To confirm the latter observation, XPS core-level spectra of FePt NPs synthesized under standard conditions were obtained, and these are shown in Figure 6. As can be seen in Figure 6f, the Fe 2p core levels are split into $2p_{1/2}$ and

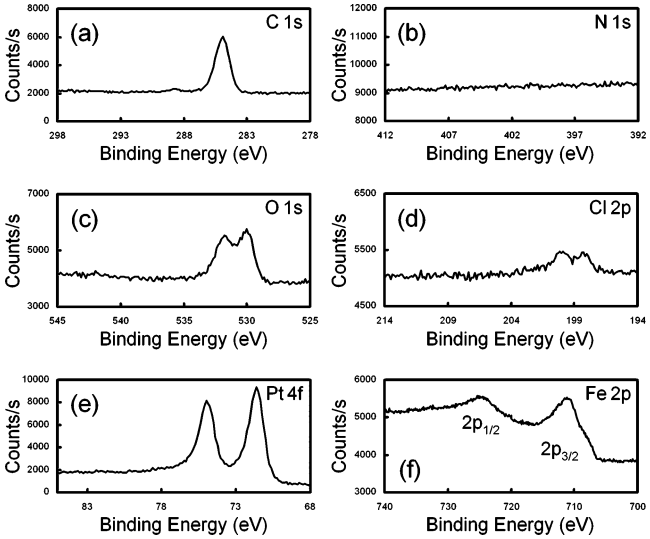

Figure 6. XPS core-level spectra of FePt NPs synthesized under standard conditions. (a) C 1s, (b) N 1s, (c) O 1s, (d) Cl 2p, (e) Pt 4f, and (f) Fe 2p peaks are plotted. The Fe 2p core levels are split into $2p_{1/2}$ and $2p_{3/2}$ components. The Pt 4f peaks are also split into two spin−orbit doublets at binding energies of 71.6 and 75 eV.

$2p_{3/2}$ components, which is due to spin−orbit coupling. In the spectrum, there is a clear shoulder on the right of the Fe $2p_{3/2}$ line shape. The Fe $2p_{3/2}$ line shape can be divided into two peaks: One is at a binding energy of 711 eV and corresponds to Fe—O, Fe—OOH, or Fe_2O_3 bonds.[18] The other is at a binding energy of 708 eV, which corresponds to pure Fe.[9,18] At the same time, the C 1s peak is observed at a binding energy of 285 eV (Figure 6a), which corresponds to C—C or C—H bonds,[18,19] and the O 1s peak is observed at a binding energy of 532 eV (Figure 6c), which corresponds to C═O bonds.[18] On the other hand, no N 1s peak was observed (Figure 6b). These results indicate that FePt NPs are capped with oleic acid molecules, and no oleylamine is present on the NP surfaces. Note that a weak Cl 2p peak was observed (Figure 6d) as a result of impurities in $Fe(OEt)_3$. The Pt 4f peaks were also split into two spin−orbit doublets at binding energies of 71.6 and 75 eV (Figure 6e). The Pt $4f_{7/2}$ binding energy (71.6 eV) is slightly higher than that of a bulk Pt sample (71.0 eV).[18] The energy shift observed in these spectra compared to the reference data for bulk Pt is due to the initial- and final-state effects of the electron emission process in small particles.[9] Thus, the former peak (71.6 eV) is attributed to the neutral state of Pt. This indicates that there is no capping agent coordinated to the Pt sites.

We have previously confirmed that the intensity of the oxygen peak in a TEM-EDX spectrum of a single NP is similar to the background level,[15] suggesting that the peak at a binding energy of 711 eV in the Fe $2p_{3/2}$ line shape (Figure 6f) indicates Fe−oleic acid coordination. Oleic acid molecules are known to form a stable covalent attachment

(18) Wagner, C. D., Muilenberg, G. E., Eds. *Handbook of x-ray photoelectron spectroscopy, a reference book of standard data for use in x-ray photoelectron spectroscopy*; Perkin-Elmer Corp., Physical Electronics Division: Eden Prairie, MN, 1979.
(19) (a) Fu, X.; Wang, Y.; Wu, N.; Gui, L.; Tang, Y. *J. Colloid Interface Sci.* **2001**, *243*, 326. (b) Li, Z. W.; Zhu, Y. F. *Appl. Surf. Sci.* **2003**, *211*, 315.

to an iron oxide surface.[20] Additionally, Rocchiccioli-Deltcheff et al. have proven that the carboxylate group adsorbs primarily via a chelating bidentate configuration to a single surface Lewis acid Fe^{3+} species on the surfaces of magnetite particles, with the IR bands appearing at ~1520 cm^{-1} [$\nu_{as}(CO_2^-)$] and 1425 cm^{-1} [$\nu_s(CO_2^-)$].[21] In their work a vibrational energy band was also observed at 1560−1580 cm^{-1}, which was attributed to an oleate bridging in a bidentate configuration.[21]

On decreasing $O_{ac}/(O_{ac} + O_{am})$ from 1 to 0.5, D_p increased and σ decreased, as shown in Figure 5, parts b, c, and d. In addition, the Fe content of NPs increased with decreasing $O_{ac}/(O_{ac} + O_{am})$ ratios. The degree of supersaturation of Fe was expected to increase, because the concentration of stabilizer (oleic acid) decreased. If the formation of NPs is dominated by the nucleation of Fe atoms, D_p should decrease with decreasing $O_{ac}/(O_{ac} + O_{am})$ ratios. However, the experimental results show the reverse trend. Hence, it is suggested that the formation of NPs was dominated by the nucleation of Pt atoms, because the effect of crystal growth on the change in D_p was slight in this reaction system, as mentioned above. If this is the case, the increase in D_p with an increasing fraction of O_{am} indicates that the Pt atoms are stabilized by the presence of oleylamine. The interaction of amine molecules with Pt is well-established in the literature.[22] In addition, Kumar et al. carried out TG analysis of a purified powder of Pt NPs capped with octadecylamine (ODA) and revealed that ODA-capped Pt NPs undergo an overall weight loss of ~30% at 255 °C, due to the desorption/decomposition of ODA molecules bound to Pt NPs, indicating that the interaction between ODA and Pt is quite strong.[23] Because the reaction temperature in our synthetic route is much higher, the strength of the interaction between oleylamine and the Pt atom could be weakened in comparison to the Fe−oleic acid bonding strength, because oleylamine is a monodentate ligand while oleic acid is a bidentate ligand. This might explain why no N 1s peak was observed by XPS analysis.

When the relative amount of O_{am} is increased, that is, when the $O_{ac}/(O_{ac} + O_{am})$ ratio is decreased, the stabilization of Pt atoms leads to a decrease in the degree of supersaturation of Pt atoms, and, therefore, the size of the Pt nucleus increases. On the other hand, the Fe atoms become destabilized, because the relative amount of oleic acid has decreased. This leads to an increase in the degree of supersaturation of Fe atoms, and, thus, the growth rate of Fe increases. As mentioned previously, because crystal growth affects σ even if the growth rate is too small to affect D_p, a significant reduction in σ might be observed with decreasing $O_{ac}/(O_{ac} + O_{am})$ ratios as shown in Figure 5f. The growth of Fe would contribute to the increased Fe content of the NPs and also slightly to the increase in D_p. According to this scenario, we can now explain the result for $O_{ac}/(O_{ac} + O_{am}) = 1$ as follows: the Fe atoms are stabilized considerably due to the presence of a large amount of oleic acid in the reaction system, while the Pt atoms are noticeably destabilized because of the absence of oleylamine. As a result, ultrafine Pt nuclei are generated, and Fe atoms are subsequently included in the Pt nuclei via a slow crystal growth process. Thus, ultrasmall Pt-rich FePt NPs are formed.

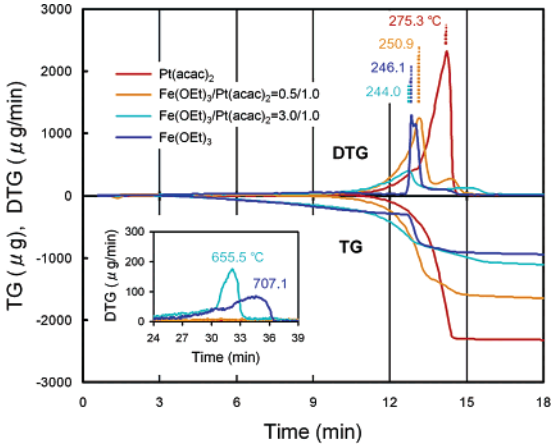

Figure 7. TG and DTG curves of $Fe(OEt)_3$ (blue), $Pt(acac)_2$ (red), a $Fe(OEt)_3/Pt(acac)_2$ mixture with a 0.5/1 molar ratio (orange), and a $Fe(OEt)_3/Pt(acac)_2$ mixture with a 3/1 molar ratio (light blue). The inset shows the DTG curves at higher temperatures.

On further decreasing the $O_{ac}/(O_{ac} + O_{am})$ ratio to 0.25, D_p and σ increased drastically, as shown in Figure 5a,f. Additionally, the shape of FePt NPs was irregular and completely different from the other cases, as shown in Figure 5a. This might be because homogeneous nucleation of Fe NPs took place as a result of excessive destabilization of Fe atoms that then agglomerated on the Pt NPs or because heterogeneous nucleation of Fe NPs on Pt NPs took place. Curves 1, 2, and 3 in Figure 2d represent the XRD patterns of the FePt NPs synthesized with $O_{ac}/(O_{ac} + O_{am}) = 0.25$, 0.5 (standard condition), and 0.67, respectively. The values of D_{xrd} were 3.82, 2.87, and 3.05 nm, and the ratios of D_{xrd} to D_p were calculated to be 0.56, 0.7, and 0.74, respectively. The considerable reduction in D_{xrd}/D_p when $O_{ac}/(O_{ac} + O_{am}) = 0.25$ indicates that the crystallinity of NPs in this sample was very different from that in the other cases, supporting the idea that Fe nucleation takes place.

In summary, we propose that (i) Fe forms a complex with oleic acid and Pt forms a complex with oleylamine. Then, (ii) FePt NPs are formed via nucleation of Fe and Pt atoms which do not form complexes with either oleic acid or oleylamine molecules. Finally, (iii) oleic acid selectively binds to the Fe sites on the NP surfaces, because the complexation strength of Fe−oleic acid might be greater at higher temperatures than that of Pt−oleylamine. Hence, no oleylamine is present on the NP surfaces.

Decomposition Behavior of Precursors. To determine the decomposition behavior of the precursors ($Fe(OEt)_3$ and $Pt(acac)_2$), to determine what could be happening to these precursors during the pyrolysis reaction, TG-DTA and TG-MS analyses of $Fe(OEt)_3$, $Pt(acac)_2$, and their mixtures were carried out. Figure 7 shows TG and differential thermogravi-

(20) Lesnikovich, A. E.; Shunkevich, T. M.; Naumenko, V. N.; Vorobyova, S. A.; Baykov, M. W. *J. Magn. Magn. Mater.* **1990**, *85*, 14.
(21) Rocchiccioli-Deltcheff, C.; Franck, R.; Cabuil, V.; Massart, R. *J. Chem. Res.* **1987**, *5*, 126.
(22) (a) Pregosin, P. S.; Omura, H.; Venand, L. M. *J. Am. Chem. Soc.* **1973**, *95*, 2047. (b) Romeo, R.; Arena, G.; Scolaro, L. M.; Plutino, M. R.; Bruno, G.; Nicol, F. *Inorg. Chem.* **1994**, *33*, 4029.
(23) Kumar, A.; Joshi, H. M.; Mandale, A. B.; Srivastava, R.; Adyanthaya, S. D.; Pasricha, R.; Sastry, M. *J. Chem. Sci.* **2004**, *116*, 293.

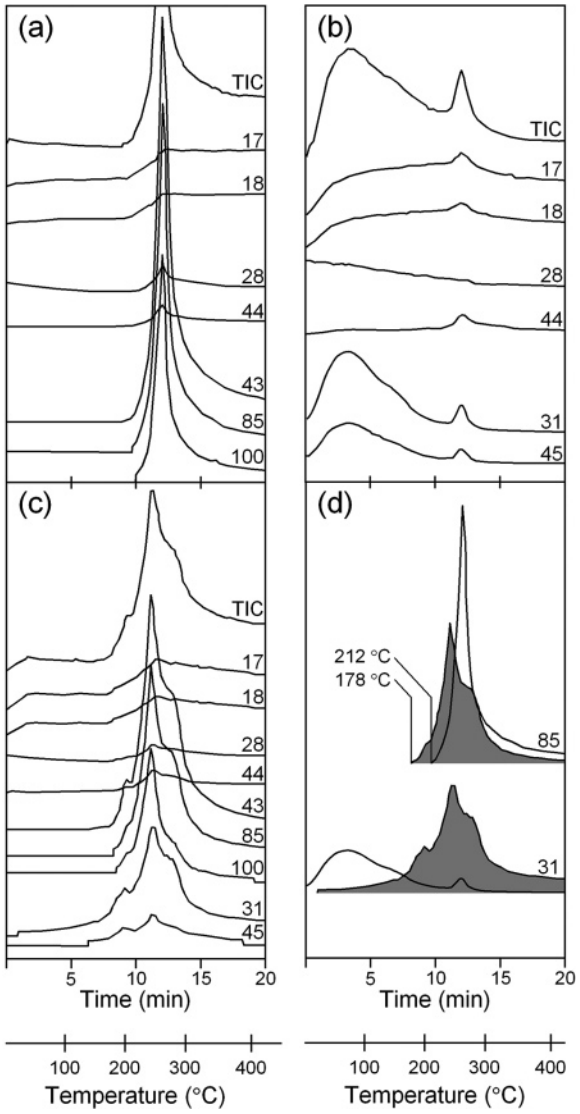

Figure 8. TG-MS spectra of (a) $Pt(acac)_2$, (b) $Fe(OEt)_3$, and (c) a $Fe(OEt)_3/Pt(acac)_2$ mixture with a 1/1 molar ratio (sample B). (d) TG-MS spectra of the acetylacetone-derived fragments (85) and the ethanol-derived fragments (31) obtained from $Pt(acac)_2$ and $Fe(OEt)_3$ (no shading under the lines) and sample B (shading under the lines) are shown on the same plots for comparison. The top curves in parts a, b, and c represent the total ion chromatograms.

metric (DTG) curves of the precursors. In the case of $Fe(OEt)_3$ (blue lines in Figure 7), weight loss started early in the process (at ~ 60 °C) and continued steadily until shortly after 12 min (~ 240 °C), at which point the weight loss accelerated rapidly and subsequently stopped; the DTG peak was at 246.1 °C. Note that the TG curves of as-received and recrystallized $Fe(OEt)_3$ (as-received $Fe(OEt)_3$ was dissolved in ethanol and dried) differed slightly, probably due to differing crystal conditions. As shown in Figure 8b, TG-MS analysis revealed that the main decomposition product of $Fe(OEt)_3$ was ethanol (with *m*/*z* values of 45 and 31; >90%; peak at ~ 260 °C). CO_2 (*m*/*z* 44 and 28) and H_2O (*m*/*z* 18 and 17) were also detected. β-Hydride elimination is a well-known reaction in the thermal decomposition of late transition metal alkoxides.[24] In the case of $Fe(OEt)_3$, a β-hydrogen in one ethoxide ligand would be transferred to the Fe atom, followed by coordination of the H-lacking ethoxide residue (acetaldehyde) onto the Fe atom and elimination of one ethanol molecule. Because the β-hydride elimination is a multistep process,[25] the drastic increase in the decomposition rate at the latter stage (~240 °C) could be due to changes in the form of the Fe complex. In the case of $Pt(acac)_2$ (red lines in Figure 7), however, the weight loss started at ~ 200 °C, and the DTG peak was found to be at 275.3 °C. The main decomposition product of $Pt(acac)_2$ was found to be acetylacetone (molecular mass 100) as shown in Figure 8a (peak at ~262 °C). Note that the TG-MS spectra of molecules with *m*/*z* values of 85 and 43 were fragments of acetylacetone.

By simultaneously dissolving $Fe(OEt)_3$ and $Pt(acac)_2$ in ethanol and then drying the solution, we obtained a uniformly blended mixture of $Fe(OEt)_3$ and $Pt(acac)_2$. We prepared three mixture samples with 0.5/1.0 (sample A), 1.0/1.0 (sample B), and 3.0/1.0 (sample C) $Fe(OEt)_3/Pt(acac)_2$ molar ratios and analyzed them by TG-DTA and TG-MS. The TG and DTG curves of samples A (orange lines) and C (light blue lines) are shown in Figure 7. The DTG peaks were shifted toward lower temperatures when the molar ratio of $Fe(OEt)_3$ to $Pt(acac)_2$ was increased. For samples A and C, the DTG peaks were at 250.9 and 244.0 °C, respectively. As shown in the inset of Figure 7, small DTG peaks were observed in sample C and the $Fe(OEt)_3$ sample at higher temperatures. These peaks correspond to the detachment of ethoxide-derived CO_2. This peak shifted toward lower temperatures when $Pt(acac)_2$ coexisted with $Fe(OEt)_3$. When the molar ratio of $Fe(OEt)_3$ to $Pt(acac)_2$ was smaller than 1/1 (sample A), the peak corresponding to CO_2 detachment disappeared.

The TG-MS spectra of sample B are shown in Figure 8c. Ethanol (*m*/*z* 45 and 31) and acetylacetone (*m*/*z* 100, 85, and 43) simultaneously detached from the mixture sample, and their peaks coincided at 242 °C, which is lower than for $Fe(OEt)_3$ by itself and $Pt(acac)_2$ by itself. Figure 8d shows a comparison of the spectra of the acetylacetone-derived fragment (85) and the ethanol-derived fragment (31) obtained from $Pt(acac)_2$ (85 only, line with no shading), $Fe(OEt)_3$ (31 only, line with no shading), and sample B (85 and 31, lines with shading underneath). The acetylacetone-derived fragment (85) started to be detected at 178 °C in the case of sample B and at 212 °C in the case of $Pt(acac)_2$. Additionally, the shoulder observed at ~262 °C in the spectra of sample B corresponded to the peak positions of ethanol and acetylacetone as observed in pure $Fe(OEt)_3$ and $Pt(acac)_2$.

On the basis of these experimental results, we propose that (i) some (or all) of the ethoxide ligands detach from $Fe(OEt)_3$ by β-hydride elimination and Fe complexes (or Fe atoms) are generated. Subsequently, (ii) Fe complexes (or Fe atoms) formed by the decomposition of $Fe(OEt)_3$ catalyze the reduction of $Pt(acac)_2$, and Pt complexes (or Pt atoms) are formed. Then, (iii) the Pt complex acts as a catalyst for the decomposition of $Fe(OEt)_3$ (or Fe complexes) and reaction i proceeds. It has been reported that Pt cations can play a critical role in inducing and accelerating the reduction

(24) Bryndza, E. H.; Calabrese, J. C.; Marsi, M.; Roe, C.; Tam, W.; Bercaw, J. E. *J. Am. Chem. Soc.* **1986**, *108*, 4805.

(25) Dongare, M. K.; Sinha, A. P. B. *Thermochim. Acta* **1982**, *57*, 37.

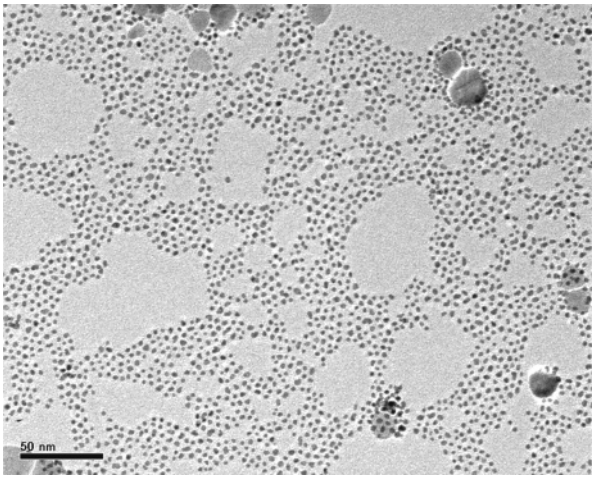

Figure 9. TEM micrographs of FePt NPs synthesized by pre-decomposition of $Fe(OEt)_3$ (see text and top curve in Figure 2a).

of associated metal cations.[26] Therefore, an Fe salt can be reduced to the neutral state when both an Fe salt and a Pt salt are simultaneously present in a system. Finally, (iv) nucleation takes place and the formation of FePt NPs occurs. In the actual reaction system, the collision frequency of the precursors (and complexes) was lower than in the mixture samples used in the thermal analyses, and the temperature at which FePt NPs were formed was higher. Consequently, the sample taken at 250 °C did not contain any FePt NPs, but contained iron oxide NPs instead (Figure 1a). The iron oxide NPs might have been formed by the oxidation of partly decomposed $Fe(OEt)_3$ during the precipitation process, followed by nucleation and growth of iron oxide.

To further investigate this process, we carried out a synthesis as follows. First, all reagents (except $Pt(acac)_2$), that is, 1.0 mmol of $Fe(OEt)_3$, 5 mmol of oleic acid, 5 mmol of oleylamine, and 14 mL of octyl ether, were put into a flask and were heated to 297 °C with a temperature ramp of 20 °C/min. Subsequently, the flask was cooled to room temperature. Second, 0.5 mmol of $Pt(acac)_2$ dissolved in 3 mL of octyl ether was put into the flask, and the reaction mixture was heated to 250 °C with a temperature ramp of 20 °C/min. A sample was taken when the temperature reached 250 °C. As mentioned above, when standard conditions in which $Fe(OEt)_3$ and $Pt(acac)_2$ were simultaneously heated in the reaction mixture were used, we did not obtain FePt NPs at 250 °C (as shown in Figures 1a and 2a). However, when $Fe(OEt)_3$ was heated above its decomposition temperature before the addition of $Pt(acac)_2$, we successfully obtained FePt NPs of $D_p = 1.9$ nm as shown in Figure 9. Curve 4 in Figure 2a corresponds to the XRD pattern of this sample, and is representative of typical fcc FePt NPs. The (311) peak due to γ-Fe_2O_3 (or Fe_3O_4) can also be seen in the XRD pattern. The large particles seen in Figure 9 might be iron oxide produced either by the oxidation of partly decomposed Fe precursors during the precipitation process, as for the sample shown in Figure 1a, or during the first heating−cooling cycle of Fe precursors in the absence of $Pt(acac)_2$. From the previous discussion, it seems reasonable to conclude that intermediates in the decomposition of $Fe(OEt)_3$ and $Pt(acac)_2$ act as catalysts for each other's decomposition reactions; that is, the decomposition of $Fe(OEt)_3$ and $Pt(acac)_2$ is allelocatalytic, and that would explain the rapid generation of FePt NPs between 250 and 297 °C.

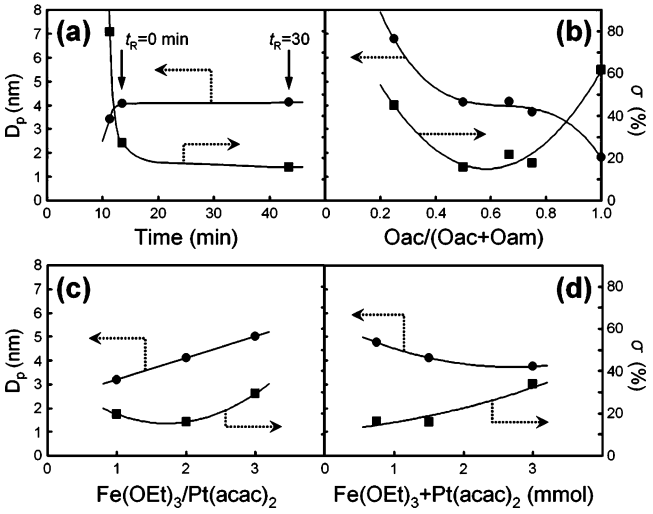

Figure 10. Average particle size D_p and size distribution σ plotted versus (a) time elapsed since the start of the temperature increase (rate of temperature increase 20 °C/min and reaction temperature 297 °C), (b) $O_{ac}/(O_{ac} + O_{am})$, (c) $Fe(OEt)_3/Pt(acac)_2$, and (d) $Fe(OEt)_3 + Pt(acac)_2$. Circles and squares represent D_p and σ, respectively.

Discussion

Our results can be summarized as follows: (i) The rate of temperature increase did not affect the formation of FePt NPs, unlike for other existing synthetic routes. (ii) The FePt NPs were formed rapidly at 250−297 °C by allelocatalytic decomposition of precursors. (iii) The formation of FePt NPs was dominated by nucleation of Pt followed by slow growth of Fe (and Pt) atoms. (iv) Fe and Pt atoms were stabilized by oleic acid and oleylamine, respectively. Figure 10 and Table 1 show a summary of the experimental results described in previous sections.

As shown in Figure 10a, the growth rates of NPs were quite small. However, the narrowing of σ is clear, suggesting that size focusing[27] has occurred as a result of the slow growth of NPs (note: the leftmost points are data for iron oxide NPs and should, therefore, be omitted). Assuming that the volume growth rate V [$m^3 \cdot s^{-1}$] does not depend on D_p [m] and that the growth is slow, the linear crystal growth rate R_g [$m \cdot s^{-1}$] can be approximated by $R_g = V/(\pi D_p^2)$. According to this equation, the smaller the D_p, the greater the R_g. This would be the basis of the size focusing in our system.

In Figure 10b, the influence of the $O_{ac}/(O_{ac} + O_{am})$ ratios on D_p and σ is shown. It can be seen that D_p increased with decreasing $O_{ac}/(O_{ac} + O_{am})$. This result indicates that the formation of FePt NPs was dominated by nucleation of Pt, as discussed in the results section. At the same time, the growth rate of Fe increased with a decreasing $O_{ac}/(O_{ac} + O_{am})$ ratio due to the destabilization of Fe. Except for when

(26) Liu, C.; Wu, X.; Klemmer, T.; Shukla, N.; Weller, D. *Chem. Mater.* **2005**, *17*, 620.

(27) Peng, X.; Wickham, J.; Alivisatos, A. P. *J. Am. Chem. Soc.* **1998**, *120*, 5343.

Table 1. Amounts of Each Reagent; Average Diameters, Size Distributions, Average Crystallite Sizes, and Average Compositions of FePt NPs; and Numbers of Pt and Fe Atoms in One NP

sample no.	$Fe(OEt)_3$ (mmol)	$Pt(acac)_2$ (mmol)	O_{ac} (mmol)	O_{am} (mmol)	D_p (nm)	σ (%)	D_{xrd} (nm)	Fe/Pt	N_{Pt}	N_{Fe}
1	1.0	0.5	5	5	4.1	16.0	2.87	50/50	1374	1374
2	1.0	0.5	2.5	7.5	6.8	44.9	3.82			
3	1.0	0.5	6.7	3.3	4.1	21.6	3.05			
4	1.0	0.5	7.5	2.5	3.7	17.8				
5	1.0	0.5	10	0	1.8	61.7	1.94	29/71	167	68
6	0.5	0.5	5	5	3.2	19.6	2.33	38/62	793	486
7	1.5	0.5	5	5	5.0	29.2	3.26	51/49	2428	2527
8	0.5	0.25	5	5	4.8	16.1	3.11	31/69	2932	1317
9	2.0	1.0	5	5	3.8	34.1	3.12	51/49	1018	1060

Scheme 1. Reaction Model for the Nucleation and Growth of FePt NPs

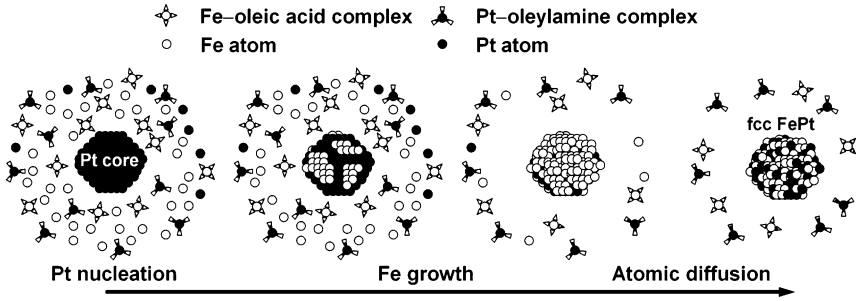

$O_{ac}/(O_{ac} + O_{am}) = 0.25$, σ decreased with a decreasing $O_{ac}/(O_{ac} + O_{am})$ ratio. This result can best be explained by the size focusing effect. By decreasing $O_{ac}/(O_{ac} + O_{am})$, that is, increasing the growth rate of Fe, the size focusing effect becomes prominent and, thus, σ decreases. The data presented in Figure 10d support that the formation of FePt NPs is dominated by the nucleation process, because the size of the nuclei increases with decreasing amounts of precursors, that is, with a decreasing degree of supersaturation. Figure 10c shows the allelocatalytic effect, that is, an increase in the level of Pt production with increasing amounts of $Fe(OEt)_3$, resulting in a large D_p and Fe content saturation.

We will now present theoretical calculations and predictions based on our proposed model (see Scheme 1) and discuss how these compare to our experimental results.

In general, the rate of nucleation R_n [$m^{-3}\cdot s^{-1}$] and the linear crystal growth rate R_g are expressed by the following equations:[28,29]

$$R_n = k_n(C - C^*)^n \quad (1)$$

$$R_g = k_g(C - C^*)^g \quad (2)$$

where k_n and k_g denote constants of nucleation and growth, respectively, C [$mol\cdot m^{-3}$] and C^* [$mol\cdot m^{-3}$] represent the actual concentration and equilibrium saturation concentration of monomer, respectively, and n and g are the orders of nucleation and growth, respectively. Normally, n is larger than g. The range of n is from 2 to 10, and the most probable values are 3−4.[29] On the other hand, the range of g is from 0 to 3, and the most probable values are 1−2.[29] Thus, the nucleation rate is more sensitive to supersaturation than the growth rate. For our experimental conditions, R_n^{Pt} is always assumed to be much larger than R_n^{Fe}, with R_n^{Pt} and R_n^{Fe} being the nucleation rates of Pt and Fe, respectively. This supposition is consistent with the fact that no N 1s peak was observed in the XPS analysis, indicating that there was no oleylamine on the FePt NP surfaces; that is, the larger coordination strength of Fe−oleic acid than that of Pt−oleylamine resulted in a larger stabilization effect and a smaller degree of supersaturation.

In addition, the mass-based nucleation rate of Fe $B^{Fe} = \pi\rho R_n^{Fe} D_0^3/6$ would be much lower than the mass-based growth rate of Fe $G^{Fe} = \int_0^\infty \pi\rho P(D_p) R_g^{Fe} D_p^2 \, dD_p$ when $O_{ac}/Fe(OEt)_3 \geq 5$. Here, D_0, ρ and $P(D_p)$ are the critical nucleus size [m], the crystal density [$mol\cdot m^{-3}$], and the number density of NPs [m^{-3}], respectively. By increasing $O_{ac}/Fe(OEt)_3$, the degree of supersaturation of Fe decreases, presumably because the concentration of Fe atoms decreases due to an increase in the concentration of Fe−oleic acid complexes according to the complexation equilibrium. Similarly, by increasing $O_{am}/Pt(acac)_2$, the supersaturation of Pt decreases. The decrease in the supersaturation of Fe leads to a decrease in the growth rate when $O_{ac}/Fe(OEt)_3 \geq 5$. On the other hand, a decrease in the supersaturation of Pt leads to a decrease in the number density of Pt nuclei, resulting in a larger Pt core.

To further verify these interpretations, the following four variables were defined as follows: $x_1 = O_{ac}/Fe(OEt)_3$, $x_2 = O_{am}/Fe(OEt)_3$, $y_1 = O_{ac}/Pt(acac)_2$, and $y_2 = O_{am}/Pt(acac)_2$. By defining $z = D_p$, one can create phase diagrams with respect to the following four sets of variables: (x_1, y_1, z), (x_1, y_2, z), (x_2, y_1, z), and (x_2, y_2, z). Among these, a distinct correlation was observed only in the case of (x_1, y_2, z). In Figure 11, we show the phase diagram for this case. Circles and polygons represent experimental data points, and their size corresponds to the D_p. Circles and polygons represent spherical and irregular shapes, respectively. The numbers in circles and polygons denote the sample numbers in Table 1. The background color represents the magnitude of D_p, which

(28) Wachi, S.; Jones, A. G. *Chem. Eng. Sci.* **1991**, *46*, 1027.
(29) Tavare, N. S. *Industrial Crystallization: Process Simulation Analysis and Design*; Plenum: New York, 1994.

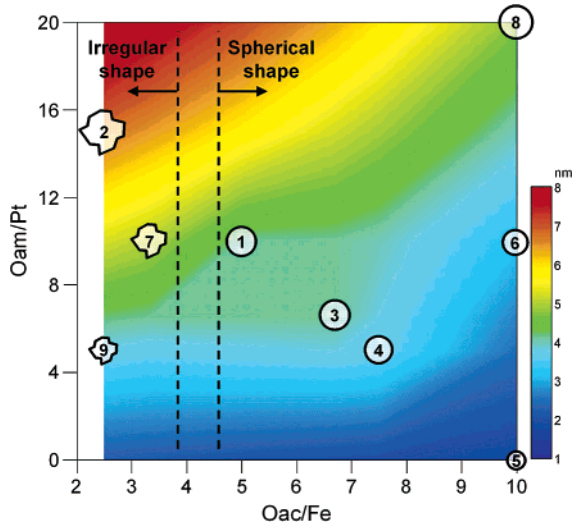

Figure 11. Average size of FePt NPs (D_p) versus $O_{ac}/Fe(OEt)_3$ and $O_{am}/Pt(acac)_2$. Circles and polygons represent experimental data points, and their sizes correspond to D_p. Circles and polygons represent spherical and irregular shapes, respectively. The numbers in the circles and the polygons denote the sample numbers in Table 1. The background color represents the magnitude of D_p, which is calculated by interpolating and extrapolating the nine experimental data points.

is calculated by interpolating and extrapolating the experimental data.

As is clearly depicted in Figure 11, D_p is a monotonically decreasing function of $O_{ac}/Fe(OEt)_3$, while it is a monotonically increasing function of $O_{am}/Pt(acac)_2$. These dependences support the premise that the formation of FePt NPs is dominated by nucleation of Pt, followed by a slow growth process of Fe atoms, where Fe and Pt atoms are stabilized by oleic acid and oleylamine, respectively. Scheme 1 illustrates this reaction model.

As shown in Table 1, the number of Pt and Fe atoms included in a single NP (N_{Pt} and N_{Fe}) was calculated from D_p and the average composition of FePt NPs by using a bulk lattice parameter of fcc-phase FePt. We will now further focus our discussion on spherical NPs. Comparing sample no. 5 with sample no. 6, N_{Pt} was found to increase with increasing $O_{am}/Pt(acac)_2$. This can be explained by the stabilization of Pt atoms and the resulting enlargement of the Pt core. The nucleation rate of the Pt core $R_{n,i}^{Pt}$ can be expressed as $R_{n,i}^{Pt} = k_n(C_i^{Pt} - C^{Pt,*})^n$ according to eq 1 where C_i^{Pt} [mol·m^{-3}] is the concentration of Pt atoms. The subscript i denotes the sample number. Assuming that the number density of Pt nuclei M_i [m^{-3}] is proportional to $R_{n,i}^{Pt}$ and that $C^{Pt,*} \approx 0$, the following relationship applies:

$$M_i \propto (C_i^{Pt})^n \tag{3}$$

Following from this, the number of Pt atoms in one nucleus is given by

$$N_{Pt,i} \approx \frac{N_A C_i^{Pt}}{M_i} \propto (C_i^{Pt})^{1-n} \tag{4}$$

where N_A is Avogadro's number. The values of $O_{am}/Pt(acac)_2$ for sample no. 5 and sample no. 6 are 0 and 10, respectively. Therefore, the number of Pt atoms available for nucleation in sample no. 5 could be larger than that in sample no. 6, that is, $C_5^{Pt} > C_6^{Pt}$. Because n is generally larger than 2,[29] we obtain the relation:

$$\frac{N_{Pt,5}}{N_{Pt,6}} = \left(\frac{C_6^{Pt}}{C_5^{Pt}}\right)^{n-1} < 1 \tag{5}$$

In fact, eq 5 is fulfilled because the experimental value of $N_{Pt,5}/N_{Pt,6}$ was 0.21. On the other hand, N_{Fe} is given by

$$N_{Fe,i} \approx \frac{N_A C_i^{Fe}}{M_i} \tag{6}$$

where C_i^{Fe} represents the concentration of Fe atoms. Thus,

$$\frac{N_{Fe,5}}{N_{Fe,6}} = \frac{C_5^{Fe}}{C_6^{Fe}}\left(\frac{C_6^{Pt}}{C_5^{Pt}}\right)^n < \frac{C_5^{Fe}}{C_6^{Fe}} \tag{7}$$

However, $C_5^{Fe}/C_6^{Fe} > 1$ because the amount of $Fe(OEt)_3$ in sample no. 5 is twice as large as that in sample no. 6 (see Table 1). Hence, we could not verify the agreement between $N_{Fe,5}/N_{Fe,6}$ and the experimental value. Now, comparing sample no. 6 with sample no. 8, N_{Pt} increases with increasing $O_{am}/Pt(acac)_2$. The values of $O_{am}/Pt(acac)_2$ for sample no. 6 and sample no. 8 were 10 and 20, respectively. Thus, the number of Pt atoms available for the nucleation in sample no. 6 could be larger than in sample no. 8, that is, $C_6^{Pt} > C_8^{Pt}$. Hence, $N_{Pt,6}/N_{Pt,8} < 1$ which is in accord with the experimental value of $N_{Pt,6}/N_{Pt,8} = 0.27$. The number of Fe atoms available for the growth in sample no. 6 is thought to be equal to that in sample no. 8, that is, $C_6^{Fe} = C_8^{Fe}$. According to eq 6, we obtain $N_{Fe,6}/N_{Fe,8} = (M_8 C_6^{Fe})/(M_6 C_8^{Fe}) = M_8/M_6$. On the basis of eq 2, $M_8/M_6 < 1$, and, therefore, $N_{Fe,6}/N_{Fe,8} < 1$. The experimental value of $N_{Fe,6}/N_{Fe,8} = 0.37$ and is in accordance with the estimated value.

Next, a comparison of sample no. 1 (standard conditions) with sample no. 6 showed that N_{Pt} increased with decreasing $O_{ac}/Fe(OEt)_3$. The values of $O_{am}/Pt(acac)_2$ for sample no. 1 and sample no. 6 were equal. Hence, $N_{Pt,1}/N_{Pt,6} \cong 1$. However, the experimental value of $N_{Pt,1}/N_{Pt,6}$ was 1.73. This discrepancy might arise because the growth rate of Pt increased according to eq 2, because $Fe(OEt)_3/Pt(acac)_2$ of sample no. 1 was larger than that of sample no. 6, and, thus, $C_1^{Pt} > C_6^{Pt}$ as a result of the allelocatalytic effect. That is, although the sizes of the Pt nuclei are almost identical in both cases, the growth rate of Pt on the Pt nuclei was enhanced for sample no. 1 compared to that for sample no. 6. As a result, the Pt intake in the FePt NPs increased. The number of Fe atoms available for growth in sample no. 1 could be larger than that in sample no. 6, that is, $C_1^{Fe} > C_6^{Fe}$. According to eq 6, $N_{Fe,1}/N_{Fe,6} = (M_6 C_1^{Fe})/(M_1 C_6^{Fe})$. Because $M_1 = M_6$ and $N_{Fe,1}/N_{Fe,6} > 1$, the experimental value of $N_{Fe,1}/N_{Fe,6} = 2.83$ is in accordance with the estimated value. Finally, we compared sample no. 1 and sample no. 5. The values of $O_{am}/Pt(acac)_2$ for sample no. 1 and sample no. 5 were 10 and 0, respectively. Thus, the number of Pt atoms available for nucleation in the case of sample no. 5 could be larger than that in the case of sample no. 1, that is, $C_5^{Pt} > C_1^{Pt}$. Hence, $N_{Pt,5}/N_{Pt,1} < 1$, which is in accordance with the experimental value $N_{Pt,5}/N_{Pt,1} = 0.12$. The number of Fe atoms available

for growth in sample no. 1 is larger than that in sample no. 5, that is, $C_1^{Fe} > C_5^{Fe}$. Therefore, $N_{Fe,5}/N_{Fe,1} = (C_5^{Fe}/C_1^{Fe})(C_1^{Pt}/C_5^{Pt})^n < 1$. The experimental value of $N_{Fe,5}/N_{Fe,1} = 0.05$, and this is in accordance with the estimated value. This agreement between the predictions based on the model and the experimental data suggests that the reaction mechanism proposed in our present study is reasonable and proper.

For irregularly shaped NPs [$O_{ac}/Fe(OEt)_3 < 4$] (Figure 11), N_{Fe} drastically increases (sample no. 7 in Table 1). The irregular shape, large σ, large discrepancy between D_p and D_{xrd}, and drastic enhancement of Fe intake support the homogeneous nucleation of Fe NPs, followed by aggregation or heterogeneous nucleation of Fe due to an excessive destabilization of Fe atoms. The critical value of $O_{ac}/Fe(OEt)_3$ for the nucleation of Fe NPs was assessed to be approximately 4.

Conclusion

To clarify the mechanism for the formation of FePt NPs synthesized via the pyrolysis of iron(III) ethoxide [$Fe(OEt)_3$] and platinum(II) acetylacetonate [$Pt(acac)_2$], we systematically investigated the variability in the average particle size D_p, the size distribution σ, and the atomic composition of NPs with changing synthetic conditions such as the reaction temperature, the rate of temperature increase, and the total amounts and input molar ratios of precursors and capping agents. TG-DTA and TG-MS analyses of $Fe(OEt)_3$, $Pt(acac)_2$, or their mixture revealed that the intermediates in the decomposition of $Fe(OEt)_3$ and $Pt(acac)_2$ act as catalysts for each other's decomposition reactions. The effects of the synthetic conditions on D_p and σ were extensively analyzed. We found the following: (i) The rate of temperature increase does not affect the formation of FePt NPs, which is unlike the case for other existing synthetic routes. (ii) FePt NPs are rapidly formed at 250−297 °C by allelocatalytic decomposition of precursors. (iii) Formation of FePt NPs is dominated by nucleation of Pt followed by a slow growth process of Fe (and Pt) atoms. (iv) Fe and Pt atoms are stabilized by oleic acid and oleylamine, respectively.

The synthetic route for FePt NPs that uses pyrolysis of $Fe(OEt)_3$ and $Pt(acac)_2$ is easy and robust enough with respect to the composition control, when compared to other existing methods. However, because the understanding of the reaction mechanisms of colloidal chemical syntheses of FePt NPs, including our synthetic method, has been insufficient up to now, it has been difficult to optimize the synthetic conditions to obtain high-quality FePt NPs. Therefore, our findings and the reaction mechanisms proposed in this study serve as a stepping stone for the further development of FePt NP syntheses.

Acknowledgment. We thank Dr. Takashima (MCRC) for performing the high-resolution TEM observations. We also thank Dr. Asatani (MCRC) for carefully reading the manuscript.

CM051760H